Near-Infrared Time-Resolved Optical Absorption Studies of the Reaction of Fully Reduced Cytochrome *c* Oxidase with Dioxygen†

Istvan Szundi, Guang-Ling Liao,‡ and Ólöf Einarsdóttir*

Department of Chemistry and Biochemistry, University of California at Santa Cruz, Santa Cruz, California 95060

Received September 21, 2000; Revised Manuscript Received December 19, 2000

ABSTRACT: Electron transfer during the reaction of fully reduced bovine heart cytochrome oxidase with dioxygen has been studied at 24 °C in the near-infrared region following photolysis of the fully reduced CO-bound complex. The transient spectral changes and kinetics were followed on microsecond to millisecond time scales at nine different wavelengths between 597 and 935 nm and were analyzed using singular value decomposition and global exponential fitting. Four apparent lifetimes, 14 μs, 40 μs, 86 μs, and 1.1 ms, were resolved. The near-infrared spectra of the intermediates are extracted on the basis of a previously proposed mechanism [Sucheta et al. (1998) *Biochemistry 37,* 17905−17914] and compared to model spectra of the postulated intermediates. The data provide a comprehensive picture of the spectral contributions of the different redox centers in their respective oxidation or ligation states in the near-infrared region and strongly support that Cu_A is partially (2/3), but not fully, oxidized in the 3-electron-reduced ferryl intermediate.

The reduction of dioxygen to water by cytochrome oxidase has been extensively studied in the Soret and visible regions by single-wavelength detection (445, 605 nm) (*1*−*4*), and more recently in our laboratory, using a gated multichannel analyzer (*5*−*7*). These studies, along with time-resolved resonance Raman (TR^3) studies (*8*−*14*), have indicated that the reaction involves the formation of compound A, followed by the putative P[1] intermediate (607 nm form), and the subsequent generation of a ferryl, F (580 nm), form. The generation of the ferryl is followed by a more rapid electron transfer between Cu_A and heme *a* (*7*).

The nature of P has been the subject of intensive discussion, and recent investigations have suggested that it is a ferryl (a_3^{4+}═O) with a radical on tyrosine 244 (*6*, *14*, *15*). This tyrosine has recently been shown by crystallographic studies to be covalently cross-linked to histidine 240, a ligand of Cu_B in the bovine heart oxidase (*16*, *17*). The formation of P has not been detected by TR^3 during the reaction of the fully reduced enzyme with dioxygen, but recent time-resolved optical absorption studies in our laboratory using a gated multichannel analyzer have suggested that P is transiently formed (*6*).

The reduction of dioxygen to water by cytochrome oxidase has also been studied at 830 nm, the putative absorbance maximum of the oxidized Cu_A (*2*, *18*, *19*), and at low temperatures in the near-infrared region (*20*−*23*). However, a comprehensive study of this reaction at room temperature in the near-infrared region has not been carried out. Moreover, the near-infrared spectral contributions of the different redox centers in their respective redox and ligation states, including those of P and F, have not been clearly established.

In this study, we have investigated the reaction of the fully reduced cytochrome oxidase with dioxygen at selected wavelengths in the near-infrared region at room temperature. Using singular value decomposition (SVD) and global exponential fitting, we have extracted the near-infrared spectra of the intermediates, including that of compound A, the putative P, and F.

MATERIALS AND METHODS

Cytochrome oxidase was isolated from bovine hearts according to the method of Yoshikawa et al. (*24*), which involves sequential ammonium sulfate fractionations in cholate and Tween. The final precipitate was dialyzed against 0.1 M sodium phosphate buffer, pH 7.4. The fully reduced form was prepared by adding sodium ascorbate and ruthenium hexammine chloride to an anaerobic oxidized enzyme solution (*5*, *6*).

The mixed-valence CO-bound enzyme was made by deoxygenating the oxidized enzyme solution with purified N_2, followed by exposure to CO until no further change at

† This work was supported by National Institutes of Health Grant GM 53788 (Ó.E.).

* Corresponding author. E-mail: olof@chemistry.ucsc.edu. Fax: 831-459-2935. Tel: 831-459-3155.

‡ Present address: Department of Molecular Physiology and Biophysics, Baylor College of Medicine, 1 Baylor Plaza, Houston, TX 77030.

[1] Abbreviations: SVD, singular value decomposition; OSMA, optical spectrometric multichannel analyzer; *b*-spectrum, spectral changes associated with a particular first-order process; Cu_A, the mixed-valence copper A center; Cu_B, copper B; a^{2+}, reduced heme *a*; a^{3+}, oxidized heme *a*; a_3^{2+}, reduced heme a_3; a_3^{3+}, oxidized heme a_3; compound A, the ferrous-oxy complex of cytochrome a_3; P, a form of the enzyme in which heme a_3 has an absorption maximum at ∼607 nm when referenced against its oxidized state; F, a ferryl (a_3^{4+}═O) form of the enzyme in which heme a_3 has an absorption maximum at ∼580 nm when referenced against its oxidized state; F_o, F in which heme *a* is oxidized, one proton is at the binuclear center, and tyrosine is deprotonated; F_I, F in which heme *a* is oxidized, one proton is at the binuclear center, and tyrosine is protonated; F_{II}, F in which heme *a* is reduced, one proton is at the binuclear center, and tyrosine is protonated.

10.1021/bi002220v CCC: $20.00
Published on Web 01/31/2001

590 nm occurred. Then ferricyanide was added to reoxidize the amount of heme *a*, which had become reduced under CO. Compound P was prepared by exposing the oxidized enzyme to CO in the presence of O_2 (*25*). The F form was made by adding excess hydrogen peroxide to an oxidized enzyme solution (*25*). The spectra of the enzyme solutions were recorded on a Perkin-Elmer Lambda 9 UV/Vis/NIR spectrophotometer in the 480−1100 nm region. The spectra which contained more than one form were fitted to a sum of the known individual spectra in the 480−700 nm region (*6*), and the spectra in the entire 480−1100 nm range were split according to the composition obtained from the fit. The concentrations of P and F were calculated on the basis of their difference spectra using extinction coefficients of 11 mM^{-1} cm^{-1} at 607−630 nm and 5.3 mM^{-1} cm^{-1} at 580−630 nm, respectively (*26*). The model difference spectra were linear combinations of ground-state spectra of the oxidized, reduced, mixed-valence CO, and fully reduced CO enzyme complexes, the spectra of the P and F derivatives, and the oxidized-minus-reduced spectrum of Cu_A. The spectrum of Cu_A is an extended version of the experimental spectrum of Cu_A from *Paracoccus nitrificans* (*27*). The spectrum at pH 7 was digitized and fitted to a sum of Gaussian curves in the respective wavelength region, 350−900 nm. The spectrum generated from the fit in the extended wavelength range, 350−1100 nm, was used as the model spectrum of Cu_A.

The fully reduced CO-bound enzyme was obtained by exposing the fully reduced enzyme to 20% CO and 80% N_2 for 30−60 min. It was mixed in a 1:1 ratio with an O_2-saturated buffer in a stopped-flow apparatus, which was interfaced to a laser photolysis system. The reaction was initiated with a 532 nm laser pulse (Nd:YAG) 400 ms after mixing. The reaction was probed at nine different wavelengths (597, 605, 615, 655, 705, 745, 795, 835, and 935 nm) using a tungsten lamp and a filter allowing only light above 580 nm through. The transmitted beam was passed through a monochromator and measured by a photodiode. To increase the light intensity reaching the photodiode, the monochromator slits were set to 2 mm, which resulted in ~30 nm bandwidth. The recorded data were corrected for the finite bandwidth of the monochromator (Appendix I). The signals were collected by a 500 MHz digitized oscilloscope (Le Croy 9350AM). Each kinetic trace was an average of 20 consecutive runs.

Data Analysis. The transient signals were recorded by the oscilloscope on a linear time scale up to ~4.5 ms. Exponential fits to linearly-spaced time points overemphasize the contribution of the late time points. To circumvent this, the time-dependent transient signals were converted to a logarithmic time scale before fitting. Each decade in the logarithmic time window was divided into 100 segments, and data points within individual segments were averaged to give a single time point. The noise in the logarithmic time plots is larger at times below 20 μs, because of the limited number of recorded points at early times. Moreover, data points below 2−3 μs may be affected by laser artifact.

The transient data were analyzed at all wavelengths and time points simultaneously using SVD and global exponential fitting as previously described (*5*, *6*, *28*, *29*). From the spectral changes (*b*-spectra) and apparent lifetimes, a mechanism was proposed from which the spectra of the reaction intermediates were determined. The derived spectra were compared to model spectra to test the validity of the proposed mechanism. Before a comparison between the intermediate and model spectra was made, the model spectra were modified in the 600−650 nm region to account for the distortion in the transient data caused by the finite bandpass of the monochromator (Appendix I).

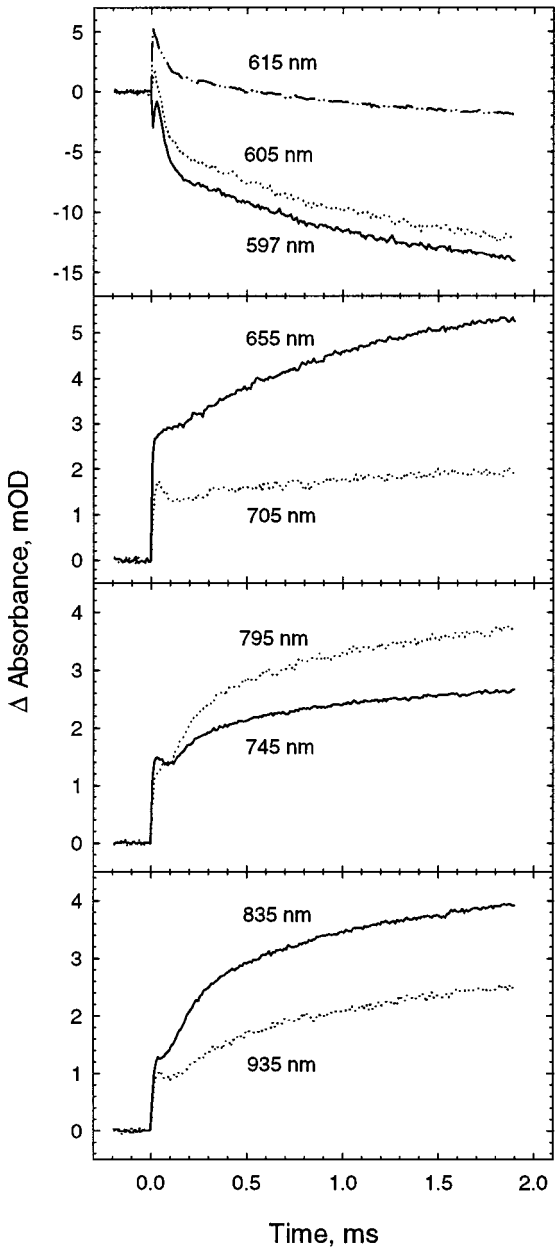

FIGURE 1: Transient absorbance changes taking place during the reduction of dioxygen to water. The transient absorbance changes are displayed on a linear time scale at nine wavelengths between 597 and 935 nm following photolysis of the fully reduced CO complex. Each kinetic trace represents the average of 20 consecutive runs. The cytochrome oxidase concentration was 6 μM before photolysis, and the effective concentration (after photolysis) was ~2 μM. The reaction was run in 0.1 M sodium phosphate buffer (pH 7.4) at 24 °C. The CO and O_2 concentrations after mixing were 0.05 atm (~50 μM) and 625 μM, respectively.

RESULTS

The transient kinetic traces for the reduction of dioxygen to water by cytochrome oxidase are shown on a linear time scale in Figure 1 at nine different wavelengths between 597

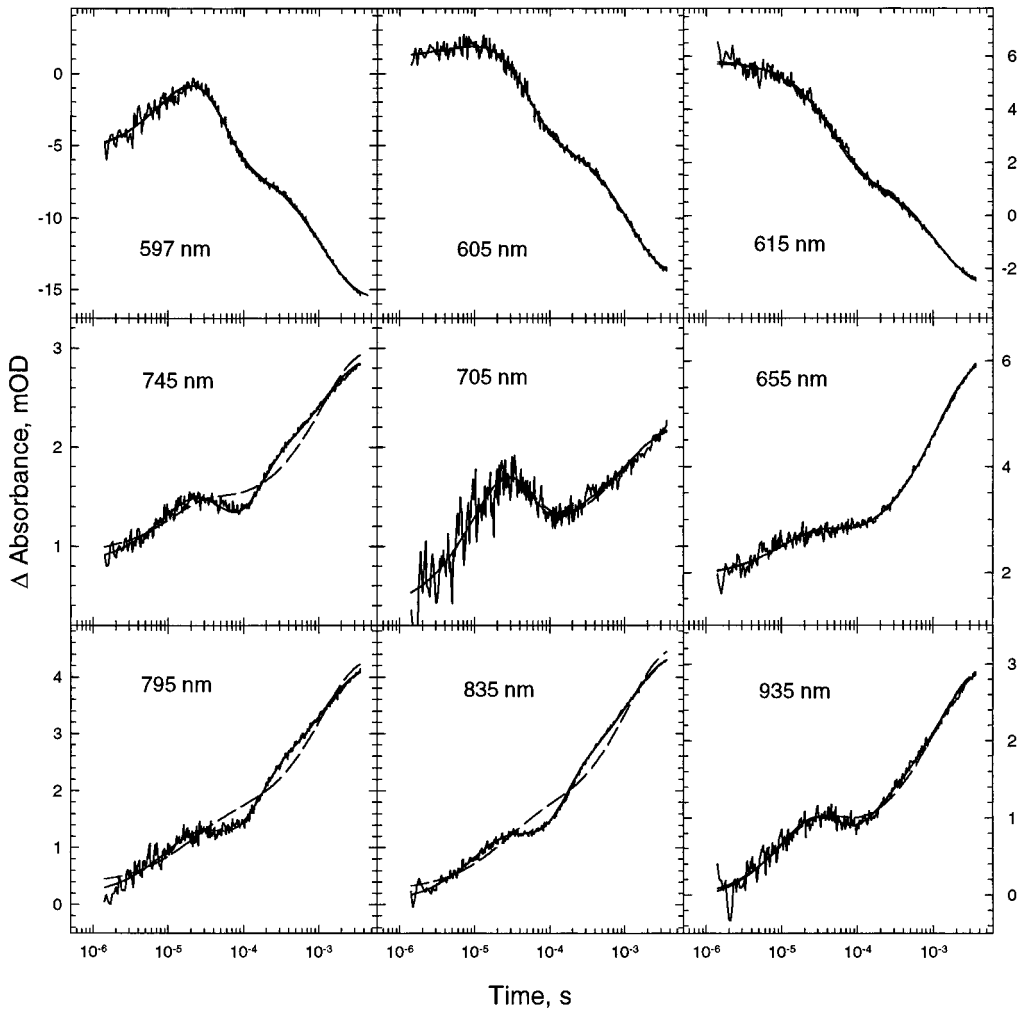

FIGURE 2: Transient kinetic traces in Figure 1 displayed on a logarithmic time scale. The conditions are the same as in Figure 1. The dashed and solid curves represent three-exponential and four-exponential fits to the transient data, respectively.

and 935 nm. For better visualization of the early time scales, the traces were truncated at 2 ms. It is clear that at least three processes are present. First a very fast process occurs, which is reflected by a rapid increase in the absorbance at 597, 705, and 745 nm, and to a lesser extent at 830 nm. This is followed by a slightly slower decay at 597 and 615 nm. A slow phase completes the reaction and is characterized by a decay in the absorbance at 597, 605, and 615 nm and increased absorbance at the other six wavelengths.

The kinetic traces, averaged on a logarithmic time scale, were represented as a two-dimensional (wavelength × delay) data matrix that was analyzed using SVD and global exponential fitting (*5*, *6*, *28*, *29*). To determine the number of processes present, the data were fitted with an increasing number of exponentials. Figure 2 shows the three-exponential (− −) and four-exponential (—) fits to the time courses at all nine wavelengths. The data are displayed on a logarithmic time scale to better separate individual processes.

The apparent lifetimes corresponding to the three-exponential fit were 13 μs, 36 μs, and 1.1 ms. The 13 μs process reflects the O_2 binding to heme a_3 (*2*, *4*, *6*, *12*). The increase at 830 nm observed upon formation of compound A is in agreement with previous single-wavelength studies at this wavelength, which reported an absorbance increase with an apparent pseudo-first-order rate constant of 1×10^5 s^{-1} ($\tau_{app} = 10$ μs) (*19*). However, this increase was attributed to O_2 binding to Cu_B^+, while we can unequivocally assign this phase to the binding of O_2 to heme a_3^{2+} based on previous experiments in both the visible and Soret regions (*5*, *6*). The 36 μs lifetime corresponds primarily to the oxidation of heme *a* (*3*, *4*, *6*, *18*, *30*, *31*), as reflected by a large spectral change (decrease) between 597 and 615 nm. Small spectral changes are observed at the other wavelengths on this time scale. The third lifetime reflects the oxidation of heme *a* on a millisecond time scale.

It is clear that an additional process (four exponentials) (Figure 2, —) is required to account for the Cu_A oxidation at 745, 795, and 835 nm. For the remaining wavelengths, the spectral changes were not optimal for reliable discrimination between the two sets. Thus, four lifetimes, 14 ± 3 μs, 40 ± 5 μs, 86 ± 30 μs, and 1.1 ± 0.2 ms, were used to fit the data. The four lifetimes represent a unique fit with a local minimum, and the lifetimes converged to the same values regardless of the initial starting values. These values are essentially the same as our previously published lifetimes (*6*). The additional 1.5 μs process, observed in our previous multichannel studies in the Soret and visible regions (*5*, *6*), was not within the time resolution of our single-wavelength detection system. It should be emphasized that the additional lifetime of 86 μs provides direct evidence for Cu_A oxidation,

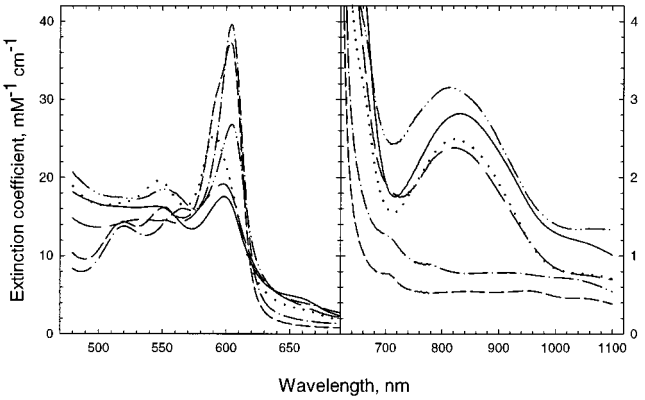

FIGURE 3: Ground-state spectra of the oxidized (—), reduced (— · —), mixed-valence CO (···), and fully reduced CO (- - -) enzyme complexes, and the spectra of the P (— ·· —) and F (— —) derivatives in the visible (left) and near-infrared region (right).

during which time small spectral changes are observed for heme *a* in the 597−615 nm spectral region. This indicates that as soon as an electron is transferred from heme *a* to heme a_3 on the millisecond time scale, heme *a* immediately gets rereduced with an electron from Cu_A.

To extract the spectra of the intermediates, a mechanism must be proposed and tested. One of the criteria for the validity of a mechanism is a good agreement between the extracted (difference) spectra of the intermediates and model spectra. The model spectra of the intermediates are generated from linear combinations of the ground-state spectra of the oxidized, reduced, mixed-valence CO, and fully reduced CO enzyme complexes, the spectra of the P and F derivatives, and the reported Cu_A difference spectrum (*27*). Figure 3 shows the ground-state spectra of these derivatives in the visible and near-infrared regions. The oxidized sample (—) has a large absorbance at 830 nm, while the reduced enzyme (— · —) and fully reduced CO-bound form (- - -) do not absorb in this region, but have an absorption band at ∼710 nm ($\epsilon = 80\ M^{-1}\ cm^{-1}$), which has been assigned to the low-spin ferrous heme *a* (*32*). The fully reduced enzyme also has a minor peak at 785 nm, which has been attributed to the unliganded five-coordinate ferrous heme a_3^{2+} (*32*−*34*) and resembles band III observed in deoxyhemoglobin and deoxymyoglobin (*35*, *36*). The mixed-valence CO enzyme (···) and the F form (— —) have almost identical spectra in the near-infrared region, resulting from the oxidized heme *a* and Cu_A, indicating that the ferryl heme a_3 (a_3^{4+}═O) has a minor contribution in this region. It is interesting to note that compound P (— ·· —) has the highest intensity in the 800−830 nm region, which may reflect the influence of the proximity of the proposed tyrosine radical on the near-infrared spectrum.

Figure 4 shows the near-infrared spectra of the oxidized-minus-reduced cytochrome oxidase (—), the oxidized-minus-reduced heme a_3/Cu_B (— · —), the oxidized-minus-reduced heme *a* (···), and the oxidized-minus-reduced Cu_A (— ·· —). It is clear that Cu_A^{2+} is responsible for 77% of the absorbance at ∼810−820 nm, while the contribution of heme *a* and heme a_3/Cu_B is 18 and 5%, respectively.

The transient data between 600 and 650 nm are distorted due to the finite monochromator band-pass. However as shown in Appendix I, we can modify the model spectra of the various intermediates to take into account this distortion.

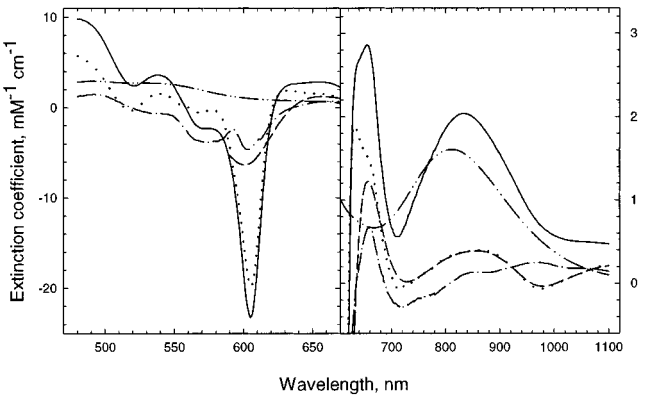

FIGURE 4: Near-infrared spectra of the oxidized-minus-reduced cytochrome oxidase (—), the oxidized-minus-reduced heme a_3/Cu_B (— · —), the oxidized-minus reduced heme *a* (···), the oxidized-minus-reduced spectrum of heme *a* modified to account for the distortion in the experimental data (- - -) and the oxidized-minus-reduced Cu_A (— ·· —).

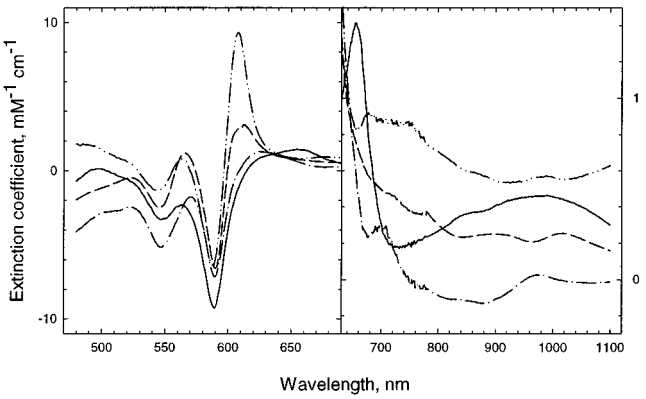

FIGURE 5: Reduced-minus-oxidized spectra of heme a_3/Cu_B in different redox and ligation states referenced against $a_3^{2+}CO\ Cu_B^+$. The spectra are the oxidized heme a_3/Cu_B ($a_3^{3+}\ Cu_B^{2+} - a_3^{2+}CO\ Cu_B^+$) (—), the reduced heme a_3 ($a_3^{2+} - a_3^{2+}CO$) (- - -), P (a_3^{4+}═O Cu_B^{2+} Tyr• − $a_3^{2+}CO\ Cu_B^+$) (— ·· —), and F (a_3^{4+}═O $Cu_B^{2+} - a_3^{2+}CO\ Cu_B^+$) (— · —).

This is necessary before a comparison between the experimentally extracted intermediate spectra and model spectra can be made in the 600−650 nm region. Figure 4 (- - -) shows how the oxidized-minus-reduced spectrum of heme *a* needs to be modified to account for the distortion in the experimental data. Similar distortion is observed in the difference spectra of the P and F forms (not shown). As discussed above and is apparent from Figure 4, this distortion is only significant in the 600−650 nm region where the amplitude changes rapidly with wavelength.

Figure 5 shows the spectra of heme a_3/Cu_B in different redox and ligation states referenced against $a_3^{2+}CO\ Cu_B^+$. These include the oxidized heme a_3/Cu_B ($a_3^{3+}\ Cu_B^{2+} - a_3^{2+}CO\ Cu_B^+$) (—), the reduced heme a_3 ($a_3^{2+} - a_3^{2+}CO$) (- - -), P (a_3^{4+}═O Cu_B^{2+} Tyr• − $a_3^{2+}CO\ Cu_B^+$) (— ·· —), and F (a_3^{4+}═O $Cu_B^{2+} - a_3^{2+}CO\ Cu_B$) (— · —). The difference between heme a_3 in the P versus F state is clearly observed. A shoulder is observed at ∼700 nm in the ferryl difference spectrum.

DISCUSSION

The kinetic analysis described here involves extracting information about the underlying mechanism and the spectra

Scheme 1: A Proposed Mechanism for the Reduction of Dioxygen to Water (*6*)

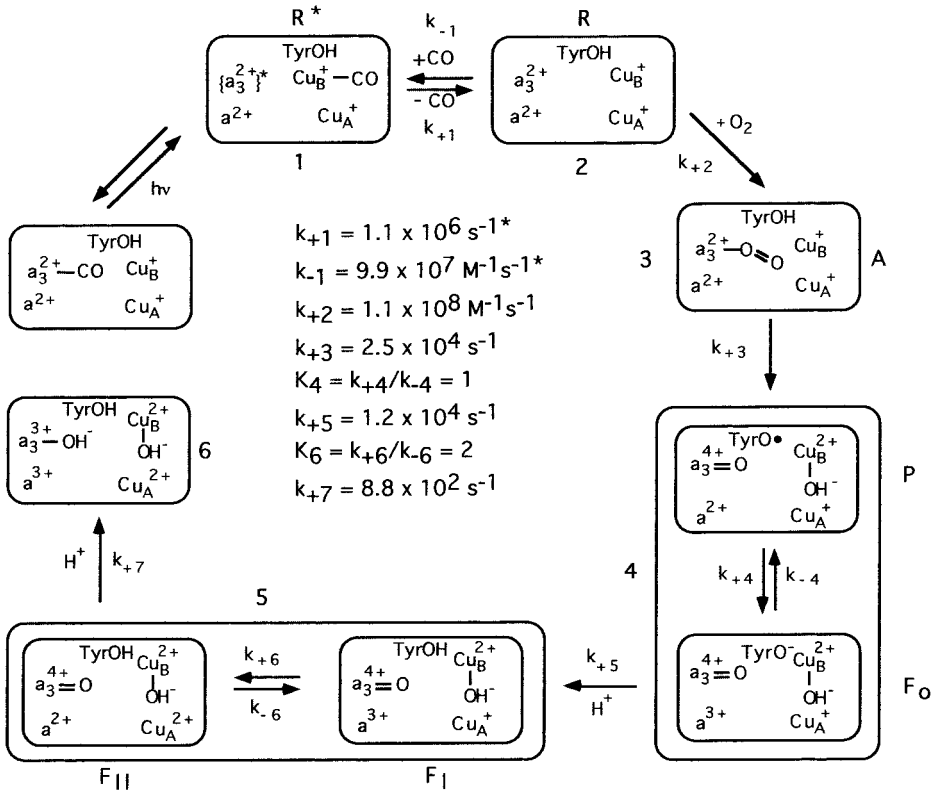

[a]Tyrosine 244, represented here as TyrOH, is postulated to function as an H-atom donor during the cleavage of the O−O bond (A → P). The rate constants k_{+1} and k_{-1} are from ref (*6*).

of the intermediates present during the reduction of dioxygen to water by cytochrome oxidase. To a first approximation, we fitted the data to the mechanism in Scheme 1, which is in accordance with our previously proposed mechanism (*6*). As discussed above, one of the criteria for the validity of a mechanism is a good agreement between the extracted spectra of the intermediates and model spectra. Another requirement is that the experimental apparent lifetimes must agree with the apparent lifetimes calculated from the microscopic rate constants (listed in Scheme 1). Because apparent lifetimes in a sequential model without back-reactions, like Scheme 1, are themselves the microscopic rate constants, only the spectral agreement was evaluated.

Intermediate Spectra. Figure 6a,b shows the model difference spectra of the intermediates (2−6) in Scheme 1 compared to the difference spectra of the intermediates extracted from the original transient data using the mechanism and the microscopic rate constants in Scheme 1. The spectra in Figures 4 and 5 form the basis for the model difference spectra of the intermediates in Scheme 1. The experimental and model spectra are referenced versus the spectrum of the fully reduced CO-bound enzyme, which has insignificant absorbance in the near-infrared region.

Our time-resolution does not allow us to extract the spectrum of intermediate 1 (R*) in Scheme 1. Intermediate 2 (Figure 6a, ●) is the reduced enzyme (R). Because we could not resolve the first process (1.5 μs) in Scheme 1 in our analysis, the first experimentally observed spectrum is really a mixture of intermediates 1 and 2 in Scheme 1. Using the reduced enzyme spectrum alone is not sufficient to account for the amplitude of the experimental absorption spectrum, but including a more red-absorbing R* (*5*, *29*) in the model spectrum (—) provides satisfactory agreement in the visible region.

We do not have a model spectrum for intermediate 3, compound A (Figure 6a, ▲), and the spectrum of the reduced CO-bound enzyme does not appropriately model that of compound A (the respective CO-difference spectrum would be zero). The dotted line for intermediate 3 represents a hypothetical spectrum of compound A based on the previously derived spectrum of this intermediate in the visible region (*6*) and on the experimental data points in the near-infrared region. It is clear that compound A has a significant absorbance in the 750−850 nm region, although not a peak, while the fully reduced CO-bound enzyme does not. It also has a small absorption band at ∼660 nm.

The exact nature of intermediate 4 is unclear, and in Figure 6b we have modeled the experimental difference spectrum (○) with P and F_o in a ratio of 1:1 (*6*). As indicated in Scheme 1, heme *a* is reduced in P and oxidized in F as previously proposed based on our data in the visible and Soret regions (*6*). Although the spectra of heme a_3 in P and F are somewhat different in the near-infrared, the small absorbance values make it difficult to reliably determine the exact redox and ligation state of the redox centers in intermediate 4.

Intermediate 5 (Figure 6b, △) is modeled assuming 70% oxidized Cu_A and 30% oxidized heme *a* (···), and this represents a good agreement with the experimental spectrum (see below). In our previous studies based on data in the visible region (*6*), we reported a ratio of 2:1 for F_{II} and F_I in intermediate 5, i.e., an equilibrium constant k_{+6}/k_{-6} of 2. This value was derived from the absorption of heme *a* since the Cu_A absorption is relatively small in the visible region. In

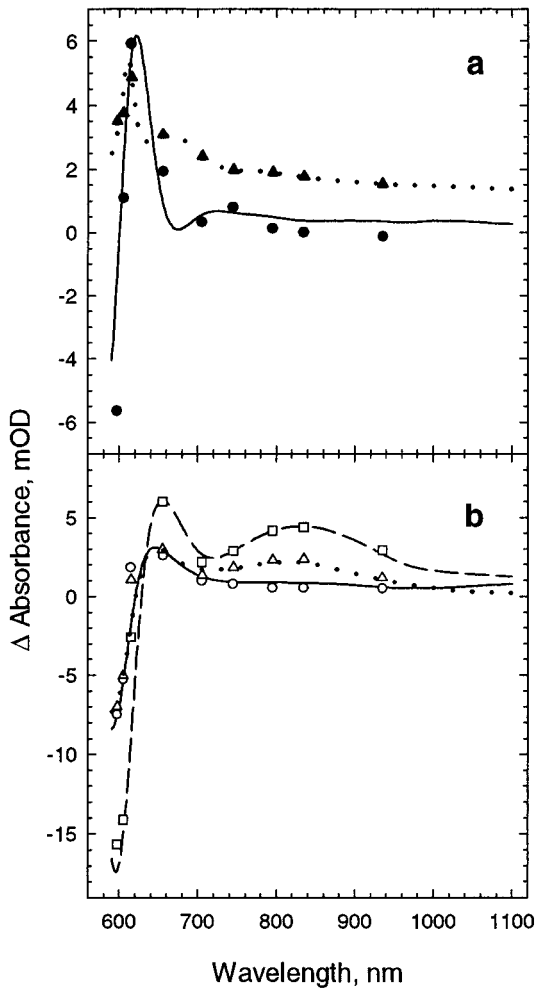

FIGURE 6: Experimental (symbols) and model (lines) spectra of the intermediates referenced versus the spectrum of the fully reduced CO-bound enzyme. Top panel: Intermediate 2 (●, −) and intermediate 3 (compound A) (▲, ···). Bottom panel: Intermediate 4 (P/F_o) (○, −), intermediate 5 (F_I/F_{II}) (△, ···), and intermediate 6 (oxidized enzyme) (□, - - -).

the study presented here, we derived the same equilibrium constant based on the absorbance in the 800 nm region, where the Cu_A absorption is dominant.

The spectrum of intermediate 6 (Figure 6b, □) is in good agreement with the model difference spectrum of the oxidized enzyme (- - -). This spectrum shows the largest absorbance at 655 nm, which has been attributed to the oxidized heme a_3/Cu_B center (*37*, *38*). It should be noted that a significant shoulder at 655 nm is not observed for the P and the F forms of the enzyme (Figure 5).

The Nature of Intermediate 4 (P/F_o). The mechanism in Scheme 1 is largely based on our previous studies in the visible and Soret regions (*6*) as well as on previous resonance Raman studies, which have provided important information regarding the structures of individual intermediates (*10*−*14*). The near-infrared studies presented here are supportive of this mechanism. The mechanism differs from that of Brzezinski and co-workers (*39*−*41*) and Wikström and co-workers (*31*, *42*) with regard to the nature of intermediate 4. Brzezinski and co-workers (*39*−*41*) and Wikström and co-workers (*31*, *42*) have postulated that intermediate 4 is P (the 607 nm form) with heme *a* being either fully oxidized (this form of the enzyme is often referred to as P_R) or close to fully oxidized (85%). This proposal is based on transient optical absorption experiments at selected wavelengths. As stated above, we have previously carried out studies in the visible and Soret regions using an intensified gated optical multichannel analyzer (*5*, *6*). This mode of detection has allowed us to monitor the reduction of dioxygen to water over a large spectral range simultaneously. Based on our multichannel studies in the visible region, intermediate 4 was first proposed to be the 607 nm species with 15% of heme *a* reduced and 85% oxidized (*5*). However, we subsequently showed that this model did not fit the data in the Soret region, while a 1:1 mixture of the 607 nm and the 580 nm species with heme *a* reduced in the former and oxidized in the latter provided a good fit in both regions (*6*). Therefore, we feel reasonably confident that intermediate 4 at pH 7.4 is not simply P in which heme *a* is oxidized, but more likely a mixture of intermediates. As discussed above, the near-infrared data on intermediate 4 presented in Figure 6b (○) cannot be used to discriminate between the two models with certainty because of the small amplitude of the signal. However, fitting intermediate 4 in the near-infrared region with a 1:1 mixture of P and F_o as shown in Scheme 1 and Figure 6b (○, −) represents a significantly better agreement than fitting intermediate 4 with the spectrum of P alone and heme *a* fully oxidized (not shown). The recent demonstration that there may be at least two compounds at the two- and three-electron-reduced state with the spectral properties of compound F (*43*, *44*) (a maximum at 580 nm in the difference spectrum) may suggest that intermediate 4 is indeed a mixture of P and F-like forms.

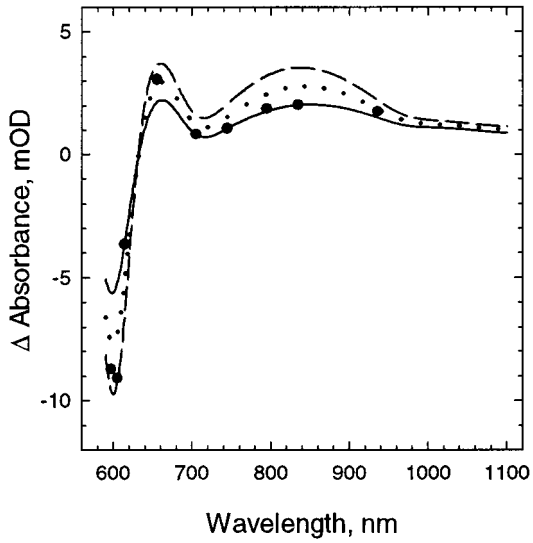

FIGURE 7: Difference between the experimental spectrum of intermediate 6 and intermediate 5 (●) and model spectra. The difference spectrum was modeled using the $a_3^{3+} - a_3^{4+}{=}O$ difference spectrum and different contributions, 0.3 (−), 0.5 (···), and 0.7 (- - -), of the oxidized-minus-reduced difference spectrum of heme $a + Cu_A$.

The Equilibrium between Cu_A and Heme a. Heme *a* and Cu_A are in a rapid redox equilibrium (*7*), which is represented by F_I and F_{II}. The portion of Cu_A oxidized in intermediate 5 can be deduced not only from modeling of this intermediate, but more easily from modeling the spectral difference between the final oxidized state, intermediate 6, and intermediate 5. This difference spectrum is shown in Figure 7 (●). The solid, dotted, and dashed curves show the modeling

of this experimental difference spectrum using the $a_3^{3+} - a_3^{4+}$=O difference spectrum + different contributions, 0.3 (—), 0.5 (•••), and 0.7 (- - -), of the (heme a + Cu_A) oxidized-minus-reduced difference spectrum. It should be emphasized that in this analysis the individual spectra of the heme *a* and Cu_A were not used, but rather the experimental oxidized (heme a + Cu_A) and the reduced (heme a + Cu_A). In the 600 nm region, in which the heme *a* contribution is predominant, the (a^{3+} minus a^{2+}) value of 0.7 provides the best fit to the experimental data. On the other hand, in the 800 nm region, the (Cu_A^{2+} minus Cu_A^{+}) value close to 0.3 gives a better fit. Thus, it is clear that upon the conversion of intermediate 5 to intermediate 6 approximately one-third of Cu_A and two-thirds of heme *a* are oxidized, consistent with an equilibrium constant k_{+6}/k_{-6} of 2.

Brzezinski and co-workers have reported that heme *a* is fully reduced in intermediate 5 in the bovine heart enzyme, while being 60% reduced in the *Rhodobacter sphaeroides* enzyme (*41*). These authors also have pointed out that the extent of electron transfer between Cu_A and heme *a* in the *Rhodobacter* enzyme appears to depend on the extent of proton uptake from the bulk solution during conversion of P to F (*45*).

Wikström and co-workers assumed an equilibrium constant, k_{+6}/k_{-6}, equal to 1 in their studies of charge translocation during a single turnover of cytochrome oxidase (*46*, *47*). This corresponds to 0.5 electron being transferred from Cu_A to heme *a* in each of the two steps, P → F and F → O. This raises the question whether the exact value of the equilibrium constant (k_{+6}/k_{-6}) makes a difference in the determination of charge translocation stoichiometries of the major electrogenic phases in the reaction of cytochrome *c* oxidase with dioxygen. However, as Wikström and co-workers have shown, the contribution of the electron transfer from Cu_A to heme *a* to the overall charge being translocated is small (*47*) (∼10 and 20% in the case of transfer of 0.5 and 1 electron from Cu_A to heme *a*, respectively), indicating that the exact value of the equilibrium constant is not crucial.

In conclusion, we have extracted the near-infrared difference spectra of the cytochrome oxidase intermediates present during the reduction of dioxygen to water at room temperature. There is an excellent agreement between the extracted intermediate spectra and model spectra using the mechanism in Scheme 1. Moreover, these data provide for the first time a comprehensive picture of the near-infrared spectra of the intermediates present during the reduction of dioxygen to water at room temperature.

APPENDIX I

Distortion of Spectra Due to a Finite Monochromator Band-Pass. Due to the narrow absorption band of the enzyme around ∼600 nm, the finite band-pass of the monochromator results in an amplitude distortion of the transient data between 600 and 650 nm. Therefore, before a comparison between the intermediate spectra extracted using a particular mechanism and model spectra can be made, the model spectra must be modified in the 600−650 nm region to account for the distortion in the transient data.

The probe intensity before laser photolysis (pre-trigger level), I_o, is equal to

$$I_o(\lambda) = I_L(\lambda) \times 10^{-A(\lambda)} \quad (1)$$

where I_L is the lamp intensity and $A(\lambda)$ is the absorbance of the sample. The probe intensity of the photolyzed sample (post-trigger), $I(\lambda)$, is equal to

$$I(\lambda) = I_L(\lambda) \times 10^{-[A(\lambda)+\Delta A(\lambda)]} \quad (2)$$

where $\Delta A(\lambda)$ is the light-induced absorbance difference. The probe intensities measured by the photodiode pre-photolysis (I_{om}) and post-photolysis (I_m) are

$$I_{om} = \sum I_o(\lambda) \times W(\lambda) \quad (3)$$

$$I_m = \sum I(\lambda) \times W(\lambda) \quad (4)$$

where $W(\lambda)$ is the relative amount of light passing through the monochromator.

One can assume a uniform lamp intensity, I_L, and a linear response of the photodiode in the band-pass window of the monochromator. The relative amount of light passing through the monochromator, $W(\lambda)$, can be approximated by a Gaussian function, with 30 nm half-width (full width at half-maximum intensity) estimated from photocurrent measurements using a He−Ne (632.8 nm) laser.

In practice, the concentration of the bleached sample is obtained from the experimental photocurrent signal where the amplitude distortion is negligible. Based on this concentration, the amplitudes of the bleached model difference spectra, $\Delta A(\lambda)$, can be determined. From the sample absorbance, $A(\lambda)$, and the band-pass, $W(\lambda)$, the distorted model spectral changes, $\Delta A_m(\lambda)$, can be calculated using eq 5:

$$\Delta A_m(\lambda) = \log (I_{om}/I_m) = \log\left(\frac{\sum 10^{-A(\lambda)} \cdot W(\lambda)}{\sum 10^{-[A(\lambda)+\Delta A(\lambda)]} \cdot W(\lambda)}\right) \quad (5)$$

It should be emphasized that the undistorted and the distorted model spectral changes are different only below 650 nm, where the absorbance of the sample changes rapidly in the monochromator band-pass window. The distortion in the spectra below 650 nm results in broader bands and a decrease in amplitude due to the integration of light intensity over a range of wavelengths.

REFERENCES

1. Greenwood, C., and Gibson, Q. H. (1967) *J. Biol. Chem. 242*, 1782−1787.
2. Oliveberg, M., Brzezinski, P., and Malmström, B. G. (1989) *Biochim. Biophys. Acta 977*, 322−328.
3. Hill, B. C. (1994) *J. Biol. Chem. 269*, 2419−2425.
4. Verkhovsky, M. I., Morgan, J. E., and Wikström, M. (1994) *Biochemistry 33*, 3079−3086.
5. Sucheta, A., Georgiadis, K. E., and Einarsdóttir, Ó. (1997) *Biochemistry 36*, 554−565.
6. Sucheta, A., Szundi, I., and Einarsdóttir, Ó. (1998) *Biochemistry 37*, 17905−17914.
7. Paula, S., Sucheta, A., Szundi, I., and Einarsdóttir, Ó. (1999) *Biochemistry 38*, 3025−3033.
8. Varotsis, C., Woodruff, W. H., and Babcock, G. T. (1989) *J. Am. Chem. Soc. 111*, 6439−6440.
9. Varotsis, C., Woodruff, W. H., and Babcock, G. T. (1990) *J. Biol. Chem. 265*, 11131−11136.
10. Han, S., Ching, Y.-C., and Rousseau, D. L. (1990) *Nature 348*, 89−90.

11. Ogura, T., Takahashi, S., Hirota, S., Shinzawa-Itoh, K., Yoshikawa, S., Appleman, E. H., and Kitagawa, T. (1993) *J. Am. Chem. Soc. 115*, 8527−8536.
12. Varotsis, C., Zhang, Y., Appleman, E. H., and Babcock, G. T. (1993) *Proc. Natl. Acad. Sci. U.S.A. 90*, 237−241.
13. Proshlyakov, D. A., Ogura, T., Shinzawa-Itoh, K., Yoshikawa, S., and Kitagawa, T. (1996) *Biochemistry 35*, 76−82.
14. Proshlyakov, D. A., Pressler, M. A., and Babcock, G. T. (1998) *Proc. Natl. Acad. Sci. U.S.A. 95*, 8020−8025.
15. Gennis, R. B. (1998) *Biochim. Biophys. Acta 1365*, 241−248.
16. Ostermeier, C., Harrenga, A., Ermler, U., and Michel, H. (1997) *Proc. Natl. Acad. Sci. U.S.A. 94*, 10547−10553.
17. Yoshikawa, S., Shinzawa-Itoh, K., Nakashima, R., Yaone, R., Yamashita, E., Inoue, N., Yao, M., Fei, M. J., Libeu, C. P., Mitzushima, T., Yamaguchi, H., Tomizaki, T., and Tsukihara, T. (1998) *Science 280*, 1723−1731.
18. Hill, B. C., and Greenwood, C. (1984) *Biochem. J. 218*, 913−921.
19. Oliveberg, M., and Malmström, B. G. (1992) *Biochemistry 31*, 3560−3563.
20. Chance, B., and Leigh, J. S. J. (1977) *Proc. Natl. Acad. Sci. U.S.A. 74*, 4777−4780.
21. Chance, B., Saronio, C., Leigh, J. S. J., Ingledew, W. J., and King, T. E. (1978) *Biochem. J. 171*, 787−798.
22. Clore, G. M., and Chance, E. M. (1978) *Biochem. J. 173*, 799−810.
23. Clore, G. M., and Chance, E. M. (1979) *Biochem. J. 177*, 613−621.
24. Yoshikawa, S., Choc, M. G., O'Toole, M. C., and Caughey, W. S. (1977) *J. Biol. Chem. 252*, 5498−5508.
25. Fabian, M., and Palmer, G. (1995) *Biochemistry 34*, 1534−1540.
26. Wikström, M., and Morgan, J. E. (1992) *J. Biol. Chem. 267*, 10266−10273.
27. Lappalainen, P., Aasa, R., Malmström, B. G., and Saraste, M. (1993) *J. Biol. Chem. 268*, 26416−26421.
28. Georgiadis, K. E., Jhon, N.-I., and Einarsdóttir, Ó. (1994) *Biochemistry 33*, 9245−9256.
29. Einarsdóttir, Ó., Georgiadis, K. E., and Sucheta, A. (1995) *Biochemistry 34*, 496−508.
30. Han, S., Ching, Y.-C., and Rousseau, D. L. (1990) *Proc. Natl. Acad. Sci. U.S.A. 87*, 8408−8412.
31. Morgan, J. E., Verkhovsky, M. I., and Wikström, M. (1996) *Biochemistry 35*, 12235−12240.
32. Einarsdóttir, Ó., Georgiadis, K. E., and Dawes, T. D. (1992) *Biochem. Biophys. Res. Commun. 184*, 1035−1041.
33. Eglinton, D. G., Johnson, M. K., Thomson, A. J., Gooding, P. E., and Greenwood, C. (1980) *Biochem. J. 191*, 319−331.
34. Ingledew, W. J., Bacon, M., and Rich, P. R. (1992) *FEBS Lett. 305*, 167−170.
35. Eaton, W. A., Hanson, L. K., Stephens, P. J., Sutherland, J. C., and Dunn, J. B. R. (1978) *J. Am. Chem. Soc. 100*, 4991−5003.
36. Eaton, W. A., and Hofrichter, J. (1981) *Methods Enzymol. 76*, 175−261.
37. Beinert, H., Hansen, R. E., and Hartzell, C. R. (1976) *Biochim. Biophys. Acta 423*, 339−355.
38. Carter, K., and Palmer, G. (1982) *J. Biol. Chem. 257*, 13507−13514.
39. Karpefors, M., Ädelroth, P., Aagaard, A., Sigurdson, H., Svensson-Ek, M., and Brzezinski, P. (1998) *Biochim. Biophys. Acta 1365*, 159−169.
40. Brzezinski, P., and Ädelroth, P. (1998) *J. Bioenerg. Biomembr. 30*, 99−107.
41. Ädelroth, P., Ek, M., and Brzezinski, P. (1998) *Biochim. Biophys. Acta 1367*, 107−117.
42. Wikström, M. (2000) *Biochim. Biophys. Acta 1458*, 188−198.
43. Fabian, M., and Palmer, G. (1995) *Biochemistry 34*, 13802−13810.
44. Jünemann, S., Heathcote, P., and Rich, P. R. (2000) *Biochim. Biophys. Acta 1456*, 56−66.
45. Karpefors, M., Ädelroth, P., Zhen, Y., Ferguson-Miller, S., and Brzezinski, P. (1998) *Proc. Natl. Acad. Sci. U.S.A. 95*, 13606−13611.
46. Verkhovsky, M. I., Morgan, J. E., Verkhovskaya, M. L., and Wikström, M. (1997) *Biochim. Biophys. Acta 1318*, 6−10.
47. Jasaitis, A., Verkhovsky, M. I., Morgan, J. E., Verkhovskaya, M. L., and Wikström, M. (1999) *Biochemistry 38*, 2697−2706.

BI002220V